RESEARCH PAPER

PCCP
www.rsc.org/pccp

Water–carbon interactions III: The influence of surface and fluid impurities

J. H. Walther,[a] T. Werder,[a] R. L. Jaffe,[b] P. Gonnet,[a] M. Bergdorf,[a] U. Zimmerli[a] and P. Koumoutsakos[a]

[a] *Institute of Computational Science, ETH Zürich, CH-8092 Zürich, Switzerland. E-mail: walther@inf.ethz.ch, werder@inf.ethz.ch, gonnetp@inf.ethz.ch, bergdorf@inf.ethz.ch, zimmerli@inf.ethz.ch and petros@inf.ethz.ch*

[b] *NASA Ames Research Center, Moffett Field, CA 94035, USA. E-mail: rjaffe@mail.arc.nasa.gov*

Received 14th October 2003, Accepted 11th March 2004
First published as an Advance Article on the web 25th March 2004

Molecular dynamics simulations are performed to study the influence of surface and fluid impurities on water–carbon interactions. In order to quantify these interactions we consider the canonical problem of wetting of a doped flat graphitic surface by a water system with impurities. As model fluid impurities we consider aqueous solutions of potassium–chloride with molar concentrations up to 1.8 M. Quantum chemistry calculations are performed to derive pair potentials for the ion–graphite interactions. The contact angle is found to decrease weakly with increasing ionic concentration, from 90° at 0 M to 81° at 1.8 M concentration. The influence of solid impurities is found to be more significant. Thus, 10, 15, and 20% coverages of chemisorbed hydrogen result in contact angles of 90°, 74° and 60°, respectively.

I. Introduction

The interaction of water with carbon surfaces is of fundamental importance for the design of nanodevices operating in aqueous environments such as carbon-nanotube based biosensors. We are conducting quantum chemistry calculations[1] and large scale molecular dynamics simulations to quantify this interaction. However as aqueous environments often contain substances such as ions and graphitic and carbon-nanotube surfaces are often doped with chemisorbed substances, it is necessary to account for the presence of such impurities when considering water–carbon interactions.

Molecular dynamics (MD) simulations provide a powerful tool for studying nanoscale fluid dynamics phenomena.[2] The atomistic description obtained from these simulations allows detailed studies of interface and surface phenomena which usually dominate at these length scales, and are not easily accessible through continuum modeling. An example from such studies is the validation of the no-slip boundary condition for carbon nanotubes operating in aqueous environments.[3] However, the ability of MD simulations to address problems in quantitative, or even qualitative agreement with relevant experiments relies critically on a number of modeling issues. These issues range from the ability of the employed interaction potentials to accurately describe the particular system, to the numerical techniques utilized to solve the governing equations. Central to the latter is the accuracy at which the non-bonded, long range van der Waals and Coulomb potentials are treated. In the first paper of this series, *cf.* Werder *et al.*[4] (subsequently denoted as WWJHK) we addressed the first issue by carefully calibrating the MD interaction potentials governing the behavior of carbon nanotubes in water by considering the related system of water wetting a graphite surface. The study demonstrated that the static contact angle of a nanometer size water droplet measured in MD simulations changes linearly with the carbon–water interaction energy, specifically the energy scale (ε_{CO}) of the carbon–oxygen Lennard-Jones potential. Thus, the macroscopic contact angle of a water droplet on a pristine graphite surface was fitted to available experimental data with an optimal value of the ε_{CO} parameter of 0.392 kJ mol^{-1}. In that study the influence from the smoothed truncation employed for the Coulomb interaction was found to be negligible as an increase of the cutoff distance form 1.0 to 2.5 nm changed the contact angle by only 1.2%. However, in the second paper of this series, *cf.* Jaffe *et al.*[5] (hereafter denoted JGWWK), the influence of the truncation, of the carbon–water Lennard-Jones interactions, was found to be non-negligible due to the inhomogeneous configuration (density) of the system. In that study, the contact angle converged to a value independent of the truncation for cutoff distances exceeding 2.0 nm, or at 1.0 nm if a continuous description through a Lennard-Jones 10–4 potential was used to describe the interaction of water molecules with each graphene layer. For these converged simulations, the recommended Lennard-Jones parameter $\varepsilon_{CO} = 0.365$ kJ mol^{-1} is 7% lower than the WWJHK value. The success of this calibration procedure relies on the availability of accurate experimental data, which for this particular system of water at a graphite surface, are rather scarce and involve a considerable variation. In 1940, Fowkes and Harkins[6] measured a contact angle of water on graphite of $85.6° \pm 0.3°$, which appears to be the value accepted in standard text books.[7] A similar value (84°) was reported by Morcos[8] who employed the rising meniscus method for water on pyrolitic graphite, and by Tadros *et al.*[9] who used the captive bubble method to find an advancing contact angle of water on graphite of 60°–80°. Schrader in 1975[10] measured contact angles of 35° and 0° for water on graphite, the latter value obtained after cleaning the surface by ion bombardment. In later experiments Schrader[11] found that ion bombardment changes the properties of the surface and finally proposed a contact angle of $42° \pm 7°$ for water on a clean, perfectly ordered graphite surface. Short exposure to air did not change the result, and Schrader ascribed the higher contact angles previously reported[6,8,9] to impurities of the surface such as chemisorption of hydrogen or contamination by hydrocarbons.[11] In more recent experiments, Luna *et al.*[12] observed

DOI: 10.1039/b312740k

 This journal is © The Owner Societies 2004

flat islands of water on graphite in scanning force microscopy studies with a maximum contact angle of 30°. However, the authors stated that possible contamination of the surface could influence their results. Similar observations were reported for the wetting properties of carbon nanotubes by Gogotsi and coworkers[13,14] who found a strong degree of wetting of aqueous solutions confined inside multiwalled carbon nanotubes. However, they later ascribed the strong wetting to OH termination of the carbon nanotube walls.[15]

In the present work we perform molecular dynamics simulations to study the influence of impurities on the contact angle of water droplets on a graphite surface. Two problems are considered. In the *first part* of this study, we consider the presence of impurities in the fluids by modeling droplets of aqueous solutions of potassium chloride in contact with a pristine graphite surface. There exists a large volume of molecular dynamics and Monte Carlo studies of ionic solutions, including dilute systems[16–25] and studies at finite concentration.[26–33] Relevant to this work area also the simulation of ions at interfaces, such as small water clusters,[34–38] and ions at planar liquid–vapor interfaces.[39–43] These studies found that the ions (Na^+, Cl^-) solvate at the liquid-vapor interface of small clusters ($N_{H_2O} < 255$),[41] but not at planar interfaces,[39] in agreement with available experiments. The threshold value for the cluster size for interior solvation was estimated to be around 500 molecules. Induced polarizability of the ions was found to have a negligible effect on the hydration,[40] whereas polarizability of the water at the interface was found to be important for the solvation of chloride in small clusters.[40] Since the droplets in the present study are relatively large (2000 water molecules), we have chosen to include polarizability in the attractive part of the potentials (*cf.* ref. 44) acting between pairs of ions, and between ions and water molecules and the carbon surface.

Studies of ions at liquid–solid interfaces are less abundant. Thus, Rose and Benjamin[45] considered the solvation of sodium chloride in water at a platinum surface. They found that while the structure of the solvation complex is very similar to that of the bulk, important differences exist in the free energy of solvation, and of the dynamics of water near the ions.

Ternary systems were studied by Uchida *et al.*[46] in molecular dynamics simulations of sodium chloride and potassium chloride mixtures at a NaCl(100) surface. The presence of a third component was found to shift the nucleation point of the binary components in agreement with experiments of aqueous solution of potassium chloride near a sodium chloride substrate *cf.* ref. 47. The effect of solvent impurities on the contact angle of droplets on graphite was recently studied by Lundgren *et al.*[48] They observed an expected reduction of the surface tension when adding methanol to the water droplet, leading to a decreased contact angle. Since potassium chloride increases the surface tension of water, this effect will increase the contact angle at higher concentrations.

In the *second part* of this study, we consider a pristine water droplet on a graphite surface randomly doped with hydrogen.[49] The stability of chemisorbed hydrogen on the basal plane of graphite was recently confirmed in *ab initio* molecular orbital studies, *cf.* ref. 50. Also, Lee and Lee[51] found hydrogen to chemisorb onto single walled carbon nanotubes in density functional theory (DFT) calculations. Similar methods were used by Jeloaica and Sidis[52] and by Miura *et al.*[53] to study the adsorption of hydrogen on graphene. They found the formation of the C–H bond forces the anchor carbon atom out of the graphene plane with a distance to the plane of 0.35 Å and with a C–H bond length of 1.13 Å. This structure of the adsorption site is used in the present study.

The paper is structured as follows: in Section II we describe the methodology and derive new pair potentials for the interaction of potassium–chloride with a graphite surface. Using similar techniques we estimate the partial charges of the C–H doping site. The results obtained for the two systems are presented in Section III and summarized in Section IV.

II. Methodology

We describe our MD simulation technique along with the details on how the contact angles and density profiles are extracted from the simulations. The parameters for the interaction potentials are those used in WWJHP supplemented with new potentials for potassium and chloride interacting with graphite. These potentials are derived from *ab initio* quantum chemistry calculations of small water–graphite systems as outlined below.

A. Interaction potentials

1. The water model and the water–carbon interaction. The water model used in this study is the rigid extended simple point charge potential SPC/E.[54] The model consists of a Coulomb potential acting between the partial point charges q on the oxygen ($-0.8476\ e$) and hydrogen ($+0.4238\ e$) atoms,

$$U_C(r_{ij}) = \frac{1}{4\pi\varepsilon_0}\frac{q_i q_j}{r_{ij}} \qquad (2.1)$$

where r_{ij} is the distance between atoms in different water molecules, and ε_{CO} is the permitivity in vacuum. The oxygens of the water molecules furthermore interact through a 12–6 Lennard-Jones potential

$$U_{12-6}(r_{ij}) = \left[\left(\frac{\sigma_{OO}}{r_{ij}}\right)^{12} - \left(\frac{\sigma_{OO}}{r_{ij}}\right)^{6}\right], \qquad (2.2)$$

with $\varepsilon_{OO} = 0.6502$ kJ mol^{-1} and $\sigma_{OO} = 3.166$ Å.[54] The SHAKE algorithm[55] is used to keep the O–H distance fixed at 1 Å and the H–O–H angle at 109.47°.

The graphite is modeled as two staggered, hexagonal carbon sheets with an inter-layer spacing of 3.4 Å. The surface is treated as a rigid structure to facilitate the sampling and to reduce the computational cost of the simulations. Thus the carbon atoms are fixed at their respective initial positions and represent an inert wall, *cf.* ref. 56. This approximate treatment of the surface was validated in WWJHP and found to have a negligible effect on the measured contact angle. The horizontal extent of the graphite is chosen sufficiently large to minimize the influence from the periodic images of the water droplet, while being computationally tractable. For the size of droplets considered in the present study with diameters of approximately 6 nm, a graphite sheet of 14×14 nm was found to provide a good compromise. The simulations for water droplets on hydrogen doped graphite are performed using truncation, which effectively removes the periodic images. Thus for these simulations, the size of the graphite sheet is reduced to 10.72×10.83 nm. Additional sheets of graphite layers were omitted from the simulations as they only contribute 2% to the total potential energy,[5] while adding considerable computational cost.

Given a particular water model, the wetting property of the fluid–solid interface is determined solely by the water–carbon interaction potential as demonstrated in WWJHP. The present study employs the potential model of WWJHP, which involves a 12–6 Lennard-Jones potential acting between the carbon and oxygen atoms of the water. The parameters of the potential are $\sigma_{CO} = 3.19$ Å and $\varepsilon_{CO} = 0.392$ kJ mol^{-1}.

2. The ion–water interaction. The potassium–water interactions are described by a 12–6 Lennard-Jones interaction between the potassium and the oxygen atom of the water and by a Coulomb potential between all charges. The ionic charges for potassium and chloride are $q_K = +1\ e$ and

$q_{Cl} = -1$ *e*, respectively. The Lennard-Jones parameters are $\sigma_{KO} = 3.260$ Å and $\varepsilon_{KO} = 0.4823$ kJ mol^{-1}, *cf.* Borodin *et al.*.[57]

The potentials governing the chloride–water interaction are taken from Smith *et al.*[44] with a 12–6 Lennard-Jones potential and a Coulomb interaction. The parameters for these potentials are $\sigma_{ClO} = 3.550$ Å, $\varepsilon_{ClO} = 0.4064$ kJ mol^{-1}. Polarization effects were found to be small for potassium–water interactions[57] and are not included in the present study.

3. The ion–carbon interaction. The interaction of charged molecules with a graphite surface is known to be enhanced by a quadrupole term centered at the graphite surface, *cf.* ref. 58. Though this interaction was found to have a negligible influence on the structural properties of water surronding carbon nanotubes,[59] it can play an important role for the structure and dynamics of ionic solutions. Thus, in the present study we have included a quadrupole term between the ions and the carbon atoms

$$U_Q(\boldsymbol{r}) = \frac{1}{3}\frac{q}{4\pi\varepsilon_0}\sum_{\alpha,\beta}\Theta_{\alpha,\beta}\frac{3r_\alpha r_\beta - r^2\delta_{\alpha\beta}}{r^5}, \qquad (2.3)$$

where α and β run over all Cartesian coordinates x,y,z and r is the distance between the ions and the quadrupole carbon site. $\delta_{\alpha\beta}$ is the Kronecker delta, and $\Theta_{\alpha,\beta}$ is the quadrupole moment tensor.[58] Eqn. (2.3) is greatly simplified when evaluated in a local coordinate system (x',y',z') centered at the quadrupole site with x' being a symmetry axis of the quadrupole, since then

$$\Theta_{x'x'} = -2\Theta_{y'y'} = -2\Theta_{z'z'}, \qquad (2.4)$$

with all other components equal to zero *cf.* ref. 58. With eqn. (2.4), eqn. (2.3) can be rewritten as

$$U_Q(\boldsymbol{r}) = C\frac{3r_x^2 - r^2}{r^5}, \text{ with } C = \frac{q\Theta_{x'x'}}{8\pi\varepsilon_0} \qquad (2.5)$$

The experimental value[58] of $\Theta_{x'x'} = -3.03 \times 10^{-40}$ C m^2 is used throughout.

To determine the total interaction energy between the ions and the graphite surface we perform *ab initio* quantum chemistry calculations of the smaller ion–graphene (benzene, naphthalene, anthracene, and pentacene) systems. The simulations are based on second order Møller–Plesset (MP2) calculations with 6-311G(2d,2p) basis sets, and all ion–graphene energies are corrected for the basis set superposition error. The calculations are carried out using the *Gaussian*98 software package.[60] The energetics of the potassium–benzene system are shown in Fig. 1 for distances between the ion and the plane of the benzene ring ranging from 2 to 5 Å. From the total potential energy we first subtract the contribution from the quadrupole term (eqn. (2.3)), and fit the remaining energy to a 10–6 Lennard Jones potential

$$U_{10-6}(r_{ij}) = \frac{25}{6}\sqrt{\frac{5}{3}}\varepsilon_{KC}\left[\left(\frac{\sigma_{KC}}{r_{ij}}\right)^{10} - \left(\frac{\sigma_{KC}}{r_{ij}}\right)^{6}\right], \qquad (2.6)$$

with the parameters $\sigma_{KC} = 2.854$ Å, and $\varepsilon_{KC} = 7.456$ kJ mol^{-1}. The energy minimum of the potential (2.6) has a value of $-\varepsilon_{KC}$ and is located at $r_{min} = \sigma_{KC}(5/3)^{(1/4)}$. In Table 1, we compare the energies of this classical potential ($U_Q + U_{10\text{-}6}$) with MP2 calculations for the larger graphene systems: benzene, naphthalene, anthracene, and pentacene. The agreement is generally good, with deviations less than 10%.

The interaction between chloride ions and carbon is determined from similar MP2 calculations of the chloride–benzene system. For the negatively charged ion the quadrupole term is purely repulsive as shown in Fig. 2. Subtracting this interaction from the total interaction energy, we are able to fit the remaining part to a 12–6 Lennard-Jones potential with the parameters $\sigma_{ClC} = 3.320$ Å and $\varepsilon_{ClC} = 1.381$ kJ mol^{-1}. By determining the ion–carbon Lennard-Jones parameters from the ion–benzene quantum chemistry calculations minus the quadrupole term, the well depth (ε) includes the contribution from the two-body ion–carbon polarization energy.

4. The ion–ion interaction. The potassium–potassium interaction is described by a 12–6 Lennard-Jones and a Coulomb interaction. The parameters for the Lennard-Jones potential are obtained by inverting the Lorentz–Berthelot mixing rules with the values for σ_{KO} and ε_{KO} from Borodin *et al.*,[57] and with the SPC/E oxygen-oxygen values. This results in $\sigma_{KK} = 3.355$ Å and $\varepsilon_{KK} = 0.3578$ kJ mol^{-1}.

The chloride–chloride interactions are obtained from ref. 44 and consist of a 12–6 Lennard-Jones interaction with $\sigma_{ClCl} = 0.4962$ Å and $\varepsilon_{ClCl} = 0.1938$ kJ mol^{-1}, a Coulomb interaction, and a polarization term to model the dipole interaction

$$U_D(r_{ij}) = \frac{D_{ClCl}}{r_{ij}^4}, \qquad (2.7)$$

with $D_{ClCl} = -0.61036$ kJ mol^{-1} nm^4.

Finally, the potassium–chloride interactions were estimated by Smith *et al.*,[44] and consist of a 12–6 Lennard-Jones potential with $\varepsilon_{KCl} = 0.2634$ kJ mol^{-1} and $\sigma_{KCl} = 0.4366$ Å,[44] a polarization term with $D_{KCl} = -0.3404$ kJ mol^{-1} nm^4, and Coulomb interactions.

5. Doped graphite. The partial charge of the chemisorbed hydrogen is estimated from *ab initio* MP2 calculation of isobutane ($(CH_3)_3CH$) and triphenylmethane ($(C_6H_5)_3CH$) using the Gaussian98 package with the 6-311G(d,p) basis set. The partial (Mulliken) charge for the hydrogen atom is 0.108 *e* and 0.142 *e* for the $(CH_3)_3CH$ and $(C_6H_5)_3CH$, respectively.

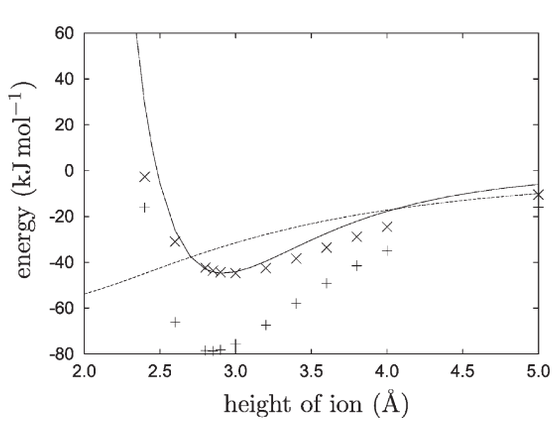

Fig. 1 MP2 calculations of the interaction energy of potassium with benzene. The quadrupole interaction (eqn. (2.3))(---) is subtracted from the total MP2 interaction energy (+++), and the remaining (×××) is fitted to a 10–6 Lennard-Jones potential (eqn. (2.6)) (—).

Table 1 Comparison of MP2 energies of potassium–graphene systems (E_{MP2}) with the corresponding energies (E_U) obtained from the derived pair potentials. The potassium ion is centered above an aromatic ring, and the *e*, and *m* superscripts denote the relative position at the edge and at the middle of the ring, respectively. *R* (in Å) is the distance of the potassium to the graphene plane. The unit of energy is kJ mol^{-1}

Substrate	*R*	E_{MP2}	E_U
Benzene	2.85	−78.12	−78.49
Naphthalene	2.80	−89.10	92.38
Anthracene^m	2.80	−97.74	−106.27
Anthracene^e	2.80	−95.48	−93.09
Pentacene^e	2.80	−102.93	−92.42

This journal is © The Owner Societies 2004

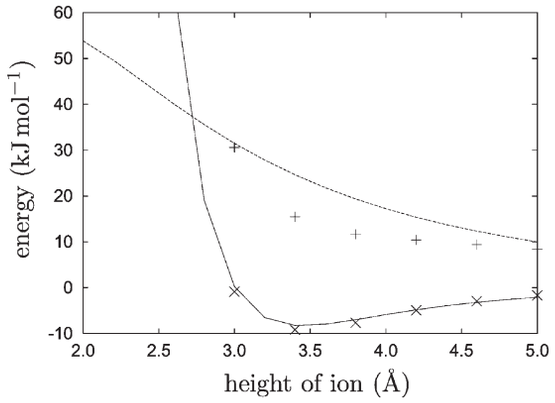

Fig. 2 MP2 calculations of the interaction energy of chloride with benzene. The quadrupole interaction, eqn. (2.3), (---) is subtracted from the total MP2 interaction energy (+++), and the remaining (×××) is fitted to a 12–6 Lennard-Jones potential, eqn. (2.2) (—).

However, for the simulations we consider a range of charges, $q_H \in [0.0\ e, 0.2\ e]$, with the corresponding negative charge on the anchoring carbon atom, thus $q_C = -q_H$. Besides this Coulombic interaction, the chemisorbed hydrogens interact through a 12–6 Lennard-Jones potential with the oxygen atoms of the water molecules. The corresponding parameters of $\varepsilon_{OH} = 0.05110$ kJ mol^{-1} and $\sigma_{OH} = 2.633$ Å are taken from the AMBER96[61] force field.

B. Numerical treatment of the non-bonded interactions

The structure and the dynamical properties of ions in solutions, specifically larger halide ions such as chloride, are known to be sensitive to the numerical treatment of the long range electrostatic interaction see *e.g.*, refs. 62 and 63. Pettitt and coworkers[64–67] found an unexpected pairing of chloride ions in dilute solutions, and similar observations were made at finite concentrations by Buckner and Jorgensen,[68] and by Vieira and Degrève.[24] While these studies used a truncation of the Coulomb interaction, simulations using reaction field and Ewald summation techniques[16,69–71] found that chloride would remain solvated. Thus, for the present simulations of aqueous solutions of potassium–chloride we employ the smooth particle mesh Ewald (SPME) technique[72] to accurately account for the long range electrostatic interactions (eqn. (2.1)). The SPME algorithm divides the $1/r$ potential into a smoothly varying part that converges fast in reciprocal space (U_{reci}) and a fast decaying, non-smooth part in real space (U_{real})

$$U_{real}(r_{ij}) = \frac{q_i q_j}{4\pi\varepsilon_0} q_i q_j \frac{\mathrm{erfc}(\alpha r_{ij})}{r_{ij}}, \qquad (2.8)$$

$$U_{reci}(r_{ij}) = \frac{q_i q_j}{4\pi\varepsilon_0} \frac{1}{\pi V} \sum_{|\vec{k}|\neq 0}^{\vec{N}_k} \frac{\exp[-(\pi|\vec{k}|\alpha)^2]}{|\vec{k}|^2} \exp(2\pi i \vec{k}\cdot\vec{r}_{ij}), \qquad (2.9)$$

where V denotes volume of the computational box. The parameter α determines the relative contribution from the two sums, and $\vec{N}_k$ is the number of wavenumbers in the reciprocal sum. To improve the computational efficiency, the latter is computed on a mesh using Fourier transforms. The parameters of the algorithm, α and $\vec{N}_k$ are adjusted to secure a converged and energy conserving solution. The cutoff distance of 1.0 nm used for the Lennard-Jones interactions and for the real part sum (eqn. (2.8)) imposes a lower limit on the α parameter. A value of 3.0 nm^{-1} was found to provide a sufficiently smooth reciprocal part with a negligible real part truncation. A mesh resolution of 64^3 grid points is used to resolve the reciprocal part of the energy (eqn. (2.9)), and corresponds to a mesh spacing of 0.22 nm in the computational box of $14 \times 14 \times 14$ nm. Using a third order B-spline interpolation for the mesh projection, the total potential energy of the system typically fluctuates less than 0.02%.

For the simulations with hydrogen doped graphite, the Coulomb interactions are computed using a smooth truncation to reduce the computational effort. Thus, eqn. (2.1) is multiplied with the smoothing function[59]

$$S(r_{ij}) = \left(1 - \frac{r_{ij}}{r_c}\right)^2, r_{ij} \leq r_c, \qquad (2.10)$$

where r_c is the cutoff radius and $S(r_{ij}) = 0$, for $r_{ij} > r_c$. The immobility and charge neutrality of the C–H pairs is expected to make this approximation acceptable. One simulation was repeated with the SPME and the contact angle changed less than 2% (from a value of 96.47° to 94.73°). The smaller charges of the dopant atoms compared with the ions also makes the truncation effects smaller.

C. Simulation parameters

The simulations in the present work are performed using the parallel molecular dynamics code FASTTUBE.[4,59,73] All simulations are carried out for 1 ns with an integration time step of 2 fs and a cutoff distance of 1.0 nm for the Lennard-Jones potentials (U_{12-6}, U_{10-6}), and a 2.0 nm cutoff for quadrupole and dipole interactions (U_Q, U_D). An overview of the simulations is shown in Tables 2 and 3. In the first half of the 200 ps equilibration time, the water is coupled to a Berendsen thermostat at a temperature of 300 K, whereas in the second half of the equilibration and for the sampling a constant energy simulation is performed. The water temperature remains stable during the production runs, *e.g.*, for case 1, it has an average of 301.8 K and a standard deviation of 3.2 K. The water molecules are initially placed on a regular lattice. For the potassium–chloride simulations two different initial configurations for the water are considered: a $4.2 \times 4.2 \times 3.0$ nm ("cubic") layout and a $5.2 \times 5.2 \times 2.0$ nm ("flat") configuration. The ions are placed within the water lattice, replacing the water molecule at that location. For each case, the number of molecules in the water lattice is adjusted to 2000 water molecules. The ionic concentration ranges from 0.0 (reference) to 1.8 M, the latter corresponding to 64 ion pairs, with intermediate

Table 2 Overview of the MD simulations of droplets of aqueous solutions of potassium chloride on graphite. N_C is the number of carbon atoms, N_{KCl} the number of ion pairs, and θ the contact angle. The number of water molecules is 2000 for all cases. The initial configuration (IC) of the water droplets is either cubic or flat. The method refers to the numerical treatment of the Coulomb interaction, which involves a smooth particle mesh Ewald (SPME) or a smooth truncation (STC)

Case	N_C	N_{KCL}	θ/°	IC	Method
1	15048	0	90.99	Cubic	SPME
2	15048	0	91.20	Flat	SPME
3	15048	0	89.73	Cubic	STC
4	15048	4	91.83	Cubic	SPME
5	15048	4	88.99	Flat	SPME
6	15048	4	88.99	Flat	STC
7	15048	8	90.77	Cubic	SPME
8	15048	8	89.23	Flat	SPME
9	15048	16	90.12	Cubic	SPME
10	15048	16	92.92	Flat	SPME
11	15048	32	88.99	Cubic	SPME
12	15048	32	87.46	Flat	SPME
13	15048	48	85.22	Cubic	SPME
14	15048	48	85.42	Flat	SPME
15	15048	64	81.41	Cubic	SPME
16	0	4	—	Cubic	SPME

Table 3 Overview of the MD simulations of water droplets on hydrogen doped graphite. The water droplets (2000 molecules) are placed on two staggered sheets of graphite containing 10 752 carbon atoms. N_H is the percentage of carbon atoms of the top layer that have a hydrogen with partial charge q_H attached to them. θ is the contact angle. The Coulomb interaction is computed using smooth truncation

Case	N_H	$\theta/^\circ$	q_H/e
17	10%	101.57	0.00
18	10%	99.51	0.05
19	10%	96.47	0.10
20	10%	89.81	0.15
21	10%	82.57	0.20
22	15%	97.15	0.00
23	15%	95.64	0.05
24	15%	87.10	0.10
25	15%	73.65	0.15
26	15%	55.96	0.20
27	20%	100.36	0.00
28	20%	98.67	0.05
29	20%	89.53	0.10
30	20%	60.26	0.15
31	20%	41.88	0.20

concentrations represented by 4, 8, 16, 32 and 48 pairs, respectively. One simulation is also performed with a droplet in vacuum to study the effect of the graphite surface (case 16). Samples of the trajectory are stored every 0.2 ps.

D. Contact angles

From the MD simulation trajectories, water isochore profiles are obtained by introducing a cylindrical binning, which uses the topmost graphite layer as zero reference level and the surface normal, through the center of mass of the droplet, as reference axis. The bins have a height of 0.5 Å and are of equal volume, *i.e.*, the radial bin boundaries are located at $r_i = \sqrt{i\delta A/\pi}$ for $i = 1, \ldots, N_{bin}$ with a base area per bin of $\delta A = 95$ Å^2. An example of a time averaged radial water density profile is shown in Fig. 3. To extract the water contact angle from such a profile, a two step procedure is adopted as described by de Ruijter *et al.*[74] and in WWJHK.[4] First, the location of the equimolar dividing surface is determined within every horizontal layer of the binned drop. Second, a circular best fit through these points is extrapolated to the graphite surface where the contact angle θ is measured.

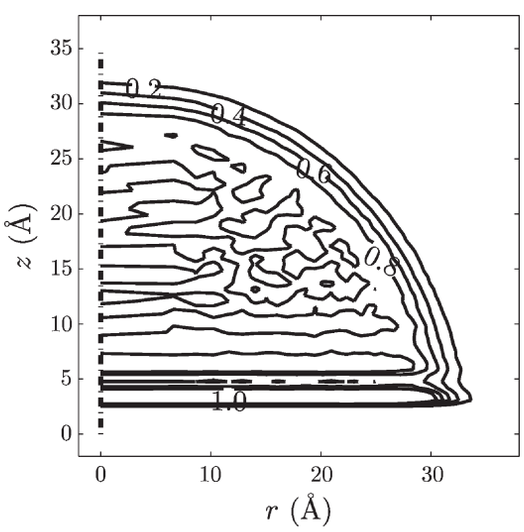

Fig. 3 The time averaged water isochore profile for case 1, *cf.* Table 2. The isochore levels are 0.2, 0.4, 0.6, 0.8, and 1.0 g cm^{-3}.

III. Results and discussion

A. Potassium–chloride droplets on graphite

Two validation studies were performed on the pristine system (zero ionic concentration) to assess the influence on the contact angle of the initial conditions (cases 1 and 2), and of the numerical treatment of the Coulomb interaction (cases 1 and 3). As demonstrated in Table 2, starting from a cubic or flat configuration of the water has little effect on the equilibrated contact angle, with a deviation less than 0.3%. Clearly, for pristine systems with an atomistically smooth surface the advancing and receeding contact angle are equal. The effect of using the smooth particle mesh Ewald (SPME) method *versus* a smooth truncation (STC) is also small with deviations less than 1.4% *cf.* Table 2, and confirms the result from WWJHK, that the contact angles obtained from simulations using a truncation of the Coulomb interaction at 1.0 nm are independent of the cutoff. The total potential energy of the three systems is −44.61, −44.66, and −43.09 kJ mol^{-1} (cases 1–3) reflecting the convergence of the simulations. The 3% lower cohesive energy obtained from the simulation using truncation is consistent with the observed (1.4%) lower contact angle as compared with the SPME simulations.

The structural properties of a droplet with four potassium chloride pairs and 2000 water molecules are presented in terms of the radial distribution function of the ions with oxygen, $g_{KO}(r)$ and $g_{ClO}(r)$, as shown in Figs. 4 and 5, respectively. For potassium, the simulation using the smooth particle mesh Ewald (SPME) and the smooth truncation are virtually identical (Fig. 4) with a limiting value of 0.5 at large distances due to the half space visible for the potassium ions located at the solid surface. Fig. 4 also compares the $g_{KO}(r)$ of the potassium ions in a water droplet (case 16) with the results of Borodin *et al.*[57] for a dilute, bulk system. The magnitude of the first peak is higher in the present simulations, with a value of 4.5 compared to 3.4 in ref. 57, but in excellent agreement with the results of Im and Roux[31] of 4.57. The location of the first and second peaks at 0.28 and 0.49 nm are in good agreement with the values of ref. 31 of 0.272 and 0.497 nm, respectively. The corresponding radial distribution for chloride–oxygen is shown in Fig. 5. Since the chloride remains solvated, all the three radial distribution functions ($g_{ClO}(r)$) converge to approximately 1.0 at large distances. The location and magnitude of the first peak are 0.34 nm and 3.2 in reasonable agreement with the values of ref. 31 of 0.312 nm and 3.97, respectively.

Snapshots from these simulations (case 4) *cf.* Fig. 6, confirm that the potassium ions have moved to the graphite surface,

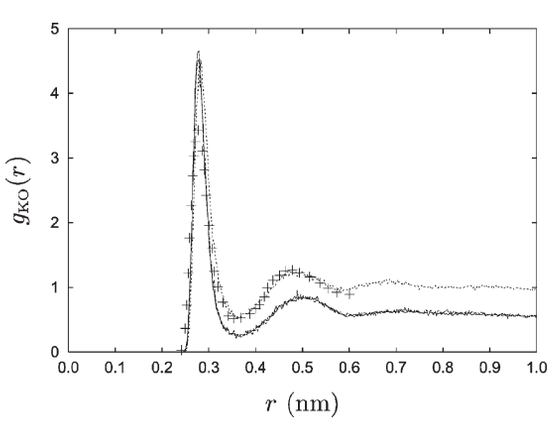

Fig. 4 Radial distribution function of K–O for the dilute solution (0.11 M). The radial distribution function obtained for the simulations using the SPME (—, case 4) and smooth truncation (---, case 6) are virtually identical. The radial distribution function for the simulation of the droplet alone (− − −, case 16) is compared with the results of Borodin *et al.*[57] (+++).

This journal is © The Owner Societies 2004

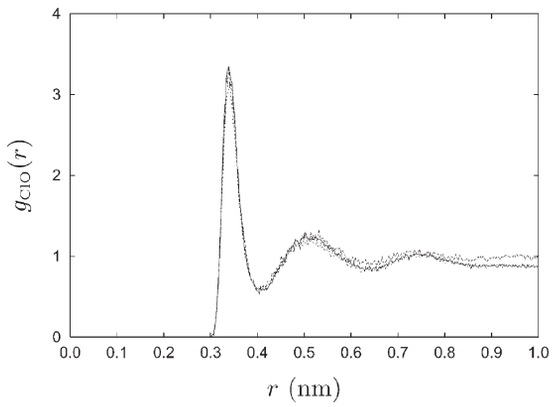

Fig. 5 Radial distribution function of C1–O for the dilute solution (0.11 M). The radial distribution function obtained for the simulations using the SPME (—, case 4) and smooth truncation (---, case 6), and for the simulation of the droplet alone (– – –, case 16).

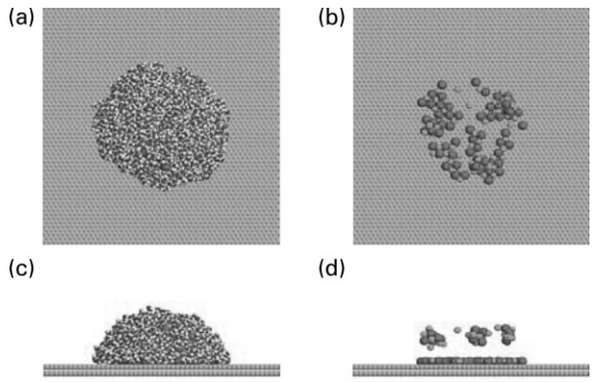

Fig. 7 Droplet of an aqueous solution of potassium–chloride at 1.8 M concentration. The droplet profile is shown in the top (a) and side views (c). The ions precipitate onto the graphite surface (b) and some form crystals at the liquid–vapor interface (d).

leaving the chloride solvated in the vicinity of the liquid–vapor interface.

The complete precipitation of potassium ions onto the graphite surface (Fig. 6d) persists at higher concentrations until the surface saturates. For the particular droplet size considered this appears to be at concentrations exceeding approximately 1 M. At higher concentrations, K–Cl clusters form at the liquid–vapor interface as shown in Fig. 7. The precipitated potassium attracts the chloride towards the graphite surface, and the simulations indicate that K–Cl surface crystals form at concentrations exceeding ≈0.5 M. As the chloride binds to the potassium at the surface, the electrostatic attraction is reduced, leaving the remaining chloride at the liquid–vapor interface to form nano-crystals at higher concentrations.

The change in contact angle with the increasing ionic concentration is small as shown in Fig. 8. Moreover, at this droplet size, the accuracy of the simulations does not allow us to measure the expected initial increase in surface tension which would lead to an increase in the contact angle. However, as the ions precipitate onto the surface, the contact angle is reduced from an initial 90° to 82° at a concentration of 1.8 M. To our knowledge, no previous modeling studies have considered the properties of K–Cl solutions on graphite surfaces.

B. Chemisorbed hydrogen on graphite

In the second part of this study we consider the influence of surface impurities on the contact angle of a pristine water droplet on graphite. As model impurity we attach hydrogen atoms at random locations anchored to the carbon atoms of the graphite surface. Simulations with a 10, 15, and 20% doping are compared with results for a pristine graphite surface. First we consider the steric effects introduced by the doping sites by assigning a zero partial charge to the doped sites, *cf.* Table 3. Due to the weak van der Waals interaction between the chemisorbed hydrogen and the water ($\varepsilon_{OH} = 0.05110$ kJ mol^{-1}), the contact angle increases slightly from a value of 89.73° for the pristine graphite surface to 101.57°, 97.15°, and 100.36° for the 10, 15, and 20% converges (cases 19, 24, and 29) *cf.* Fig. 9. At partial charges of 0.05 *e* and 0.10 *e* the contact angle reaches a value similar to the pristine surface of 96.47°, 87.10°, and 89.53°, respectively. Finally, at the partial charge predicted from *ab initio* calculations the contact angle for the high coverage is approximately 60° characteristic of a hydrophobic surface. A snapshot from the simulation with 20% doping coverage and a partial charge of 0.15 *e* is shown in Fig. 10. In conclusion, even for the weakly hydrophilic C–H surface groups considered in the present study, the influence of surface impurities on the contact angle is clearly strong. This effect should be greater for graphite surfaces with chemisorbed hydroxyl groups because the larger partial charges and the O–H bond dipole can facilitate hydrogen bond formation between water molecules and the dopant species.

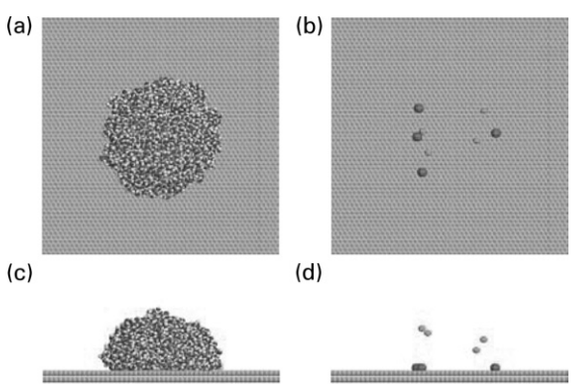

Fig. 6 The equilibrated structure of a dilute (0.11 M) droplet of potassium chloride on a graphite surface (case 4). The top view shows the circular footprint of the droplet (a), and the positions of the ions (b). The side view of the droplet (c) reveals a contact angle of ≈90°, and precipitation of the potassium ions onto the surface (d).

IV. Summary

In a series of papers, we have calibrated the interaction potentials governing the wetting behaviour of graphite and related carbon surfaces such as carbon nanotubes. The calibration

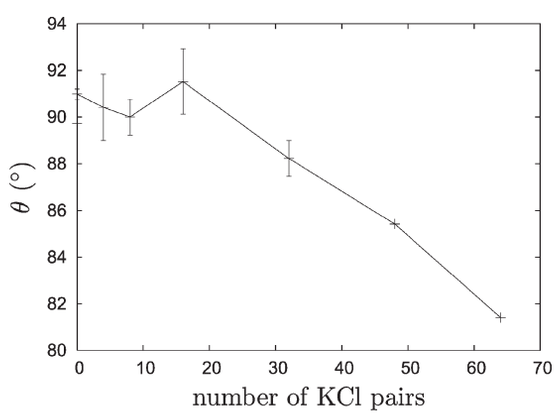

Fig. 8 Microscopic contact angle as function of the ionic concentration (number of KCI pairs).

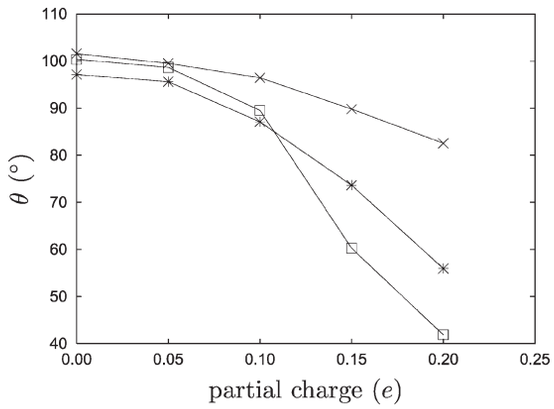

Fig. 9 Microscopic contact angle of a water droplet on graphite with chemisorbed hydrogen at 10% (×), 15% (✳), and 25% (□) coverage. The contact angle decreases with increasing the partial charge of the doped site.

has been performed using molecular dynamics simulations of pure water droplets on pristine graphite surfaces[4] to match the experimental value of the contact angle of the system. In the second paper of this series,[5] we have considered the influence of the numerical parameters and approximations employed in these simulations. The main source of error is the commonly employed truncation of the long range van der Waals interaction. In the present paper, we have considered the influence of system imperfections, such as the presence of impurities in the fluid and on the solid surfaces, on the measured contact angle of water droplets. As model impurities of the fluid we have considered aqueous solution of a potassium chloride at concentrations from 0.0 to 1.8 M. The potassium was found to precipitate onto the graphite surface and, beyond a certain concentration, to attract chloride to form a crystal layer on the graphite surface. The extent of the precipitation is mainly governed by the charge–quadrupole and the 10-6 Lennard Jones interaction of the potassium with the graphite surface. These potentials and their parameters are still subject of ongoing research and changes in these may influence the amount of precipitation at the surface. Due to the charges of the ionic surface layer the water more readily wets the surface and the contact angle is reduced by 8° to a value of 82°. The impurity considered for the graphite surface is chemisorbed hydrogen at 10, 15 and 20% coverage. The partial charges at the doping sites were determined from *ab initio* quantum chemistry calculations to be 0.142 *e*, but a range of partial charges were considered for the molecular dynamics simulations spanning the *ab initio* value. For this system the contact angle changes considerably with a value of approximately 90°, 74°, and 60° for a partial charge of 0.15 *e* and 10, 15 and 20% coverage.

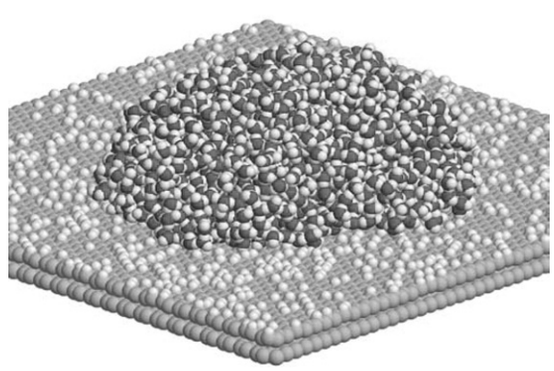

Fig. 10 Snapshot from a simulation of a water droplet on a graphite surface with a 20% coverage of chemisorbed hydrogen (case 29).

References

1 U. Zimmerli, M. Parrinello and P. Koumoutsakos, *J. Chem. Phys.*, 2004, **120**, 2693–2699.
2 P. Koumoutsakos, U. Zimmerli, T. Werder and J. H. Walther, *ASME/SPIE Handbook of Nanotechnology*, 2003.
3 J. H. Walther, T. Werder, R. L. Jaffe and P. Koumoutsakos, *Phys. Rev. E*, 2003.
4 T. Werder, J. H. Walther, R. L. Jaffe, T. Haliciogu and P. Koumoutsakos, *J. Phys. Chem. B*, 2003, **107**, 1345–1352.
5 R. L. Jaffe, P. Gonnet, T. Werder, J. H. Walther and P. Koumoutsakos, *Mol. Simul.*, 2003, **30**, 205–216.
6 F. M. Fowkes and W. D. Harkins, *J. Am. Chem. Soc.*, 1940, **62**(12), 3377–3377.
7 A. W. Adamson and A. P. Gast, *Physical Chemistry of Surfaces*, John Wiley & Sons, New York, 6th edn., 1997.
8 I. Morcos, *J. Chem. Phys.*, 1972, **57**(4), 1808–1802.
9 M. E. Tadros, P. Hu and A. W. Adamson, *J. Colloid Interface Sci.*, 1974, **49**(2), 184–195.
10 M. E. Schrader, *J. Phys. Chem.*, 1975, **79**(23), 2508–2515.
11 M. E. Schrader, *J. Phys. Chem.*, 1980, **84**, 2774–2779.
12 M. Luna, J. Colchero and A. M. Baró, *J. Phys. Chem. B*, 1999, **103**, 9576–9581.
13 Y. Gogotsi, J. A. Libera, A. Güvenç-Yazicioglu and C. M. Megaridis, *Appl. Phys. Lett.*, 2001, **79**(7), 1021–1023.
14 C. M. Megaridis, A. Güvenç-Yazicioglu, J. A. Libera and Y. Gosotsi, *Phys. Fluids*, 2002, **14**(2), L5–L8.
15 Y. Gogotsi, N. Naguib and J. A. Libera, *Chem. Phys. Lett.*, 2002, **365**, 354–360.
16 E. Guàrdia, R. Rey and J. A. Padró, *J. Chem. Phys.*, 1991, **95**(4), 2823–2831.
17 S. H. Lee and J. C. Rasaiah, *J. Phys. Chem.*, 1996, **100**, 1420–1425.
18 D. E. Smith and L. X. Dang, *J. Chem. Phys.*, 1994, **100**(5), 3757–3766.
19 L. Degrève, V. M. de Pauli and M. A. Duarte, *J. Chem. Phys.*, 1997, **106**(2), 655–665.
20 S. Koneshan, J. C. Rasaiah, R. M. Lynden-Bell and S. H. Lee, *J. Phys. Chem. B*, 1998, **102**, 4193–4204.
21 L. M. Ramaniah, M. Bernasconi and M. Parrinello, *J. Chem. Phys.*, 1999, **111**(4), 1587–1591.
22 S. Koneshan and J. C. Rasaiah, *J. Chem. Phys.*, 2000, **113**(18), 8125–8137.
23 J. Zhou, L. Xiaohua, Y. Wang and J. Shi, *Fluid Phase Equilib.*, 2002, **194–197**, 257–270.
24 D. S. Vieira and L. Degrève, *J. Mol. Struct.*, 2002, **580**, 127–135.
25 M. Carrillo-Tripp, H. Saint-Martin and I. Ortega-Blake, *J. Chem. Phys.*, 2003, **118**(15), 7062–7073.
26 A. P. Lyubartsev and A. Laaksonen, *J. Phys. Chem.*, 1996, **100**, 16 410–16 418.
27 T. Driesner, T. M. Seward and I. G. Tironi, *Geochim. Cosmochim. Acta*, 1998, **62**(18), 3095–3107.
28 T. Driesner and P. T. Cummings, *J. Chem. Phys.*, 1999, **111**(11), 5141–5149.
29 L. Degrève and F. L. B. da Silva, *J. Chem. Phys.*, 1999, **111**(11), 5150–5156.
30 L. Degrève and F. L. B. da Silva, *J. Mol. Liq.*, 2000, **87**, 217–232.
31 W. Im and B. Roux, *J. Mol. Bio.*, 2002, **319**, 1177–1197.
32 Y. Laudernet, T. Cartailler, P. Turq and M. Ferrario, *J. Phys. Chem. B*, 2003, **107**, 2354–2361.
33 L. Degrève and F. M. Mazze, *Mol. Phys.*, 2003, **101**(10), 1443–1453.
34 E. N Brodskaya and A. I. Rusanov, *Mol. Phys.*, 1990, **71**(3), 567–585.
35 L. Perera and M. L. Berkowitz, *J. Chem. Phys.*, 1991, **95**(3), 1954–1963.
36 L. Perera and M. L. Berkowitz, *J. Chem. Phys.*, 1992, **96**(11), 8288–8298.
37 L. Perera and M. L. Berkowitz, *J. Chem. Phys.*, 1993, **99**(5), 4236–4237.
38 K. J. Oh, G. T. Gao and X. C. Zeng, *Phys. Rev. Lett.*, 2001, **86**(22), 5080–5083.
39 M. A Wilson and A. Pohorille, *J. Chem. Phys.*, 1991, **95**(8), 6005–6013.
40 S. J. Stuart and B. J. Berne, *J. Phys. Chem.*, 1996, **100**, 11 934–11 943.
41 S. J. Stuart and B. J. Berne, *J. Phys. Chem. A*, 1999, **103**, 10 300–10 307.
42 P. Jungwirth and D. J. Tobias, *J. Phys. Chem. B*, 2001, **105**, 10 468–10 472.

 This journal is © The Owner Societies 2004

43 P. Jungwirth and D. J. Tobias, *J. Phys. Chem. B*, 2002, **106**, 6361–6373.
44 G. D. Smith, R. L. Jaffe and H. Partridge, *J. Phys. Chem. A*, 1997, **101**(9), 1705–1715.
45 D. A. Rose and I. Benjamin, *J. Chem. Phys.*, 1991, **95**(9), 6856–6865.
46 H. Uchida, N. Takiyama and M. Matsuoka, *Cryst. Growth Des.*, 2003, **3**(2), 209–213.
47 M. Matsuoka, K. Yamamoto, H. Uchida and H. Takiyama, *J. Cryst. Growth*, 2002, **244**, 95–101.
48 M. Lundgren, N. L. Allan, T. Cosgrove and N. George, *Langmuir*, 2002, **18**, 10 462–10 466.
49 H. P. Boehm, in *Graphite and Precursors*, ed. P. Delhaés, Gordon and Breach Science Publishers, New York, 2001, c. 7, pp. 141–178.
50 F. H. Yang and R. T. Yang, *Carbon*, 2002, **40**, 437–444.
51 S. M. Lee and Y. H. Lee, *Appl. Phys. Lett.*, 2000, **76**(20), 2877–2879.
52 L. Jeloaica and V. Sidis, *Chem. Phys. Lett.*, 1999, **300**, 157–162.
53 Y. Miura, V. Kasai, W. Diño, H. Nakanishi and T. Sugimoto, *J. Appl. Phys.*, 2003, **93**(6), 3395–3400.
54 H. J. C. Berendsen, J. R. Grigera and T. P. Straatsma, *J. Phys. Chem.*, 1987, **91**, 6269–6271.
55 J.-P. Ryckaert, G. Cicotti and H. J. C. Berendsen, *J. Comput. Phys.*, 1977, **23**, 327–341.
56 M. J. P. Nijmeijer, C. Bruin, A. F. Bakker and J. M. J. van Leeuwen, *Phys. Rev. A*, 1990, **42**(10), 6052–6059.
57 O. Borodin, R. L. Bell, Y. Li, G. D. Bedrov and Dmitry Smith, *Chem. Phys. Lett.*, 2001, **336**, 292–302.
58 F. Y. Hansen and L. W. Bruch, *Phys. Rev. B*, 1995, **51**(4), 2515–2536.
59 J. H. Walther, R. Jaffe, T. Halicioglu and P. Koumoutsakos, *J. Phys. Chem. B*, 2001, **105**, 9980–9987.
60 M. J. Frisch, G. W. Trucks, H. B. Schlegel, G. E. Scuseria, M. A. Robb, J. R. Cheeseman, V. G. Zakrzewski, J. A. Montgomery, Jr., R. E. Stratmann, J. C. Burant, S. Dapprich, J. M. Millam, A. D. Daniels, K. N. Kudin, M. C. Strain, O. Farkas, J. Tomasi, V. Barone, M. Cossi, R. Cammi, B. Mennucci, C. Pomelli, C. Adamo, S. Clifford, J. Ochterski, G. A. Petersson, P. Y. Ayala, Q. Cui, K. Morokuma, D. K. Malick, A. D. Rabuck, K. Raghavachari, J. B. Foresman, J. Cioslowski, J. V. Ortiz, A. G. Baboul, B. B. Stefanov, G. Liu, A. Liashenko, P. Piskorz, I. Komaromi, R. Gomperts, R. L. Martin, D. J. Fox, T. Keith, M. A. Al-Laham, C. Y. Peng, A. Nanayakkara, C. Gonzalez, M. Challacombe, P. M. W. Gill, B. Johnson, W. Chen, M. W. Wong, J. L. Andres, C. Gonzalez, M. Head-Gordon, E. S. Replogle and J. A. Pople, *Gaussian 98, revision A.7*, Gaussian, Inc., Pittsburgh PA, 1998.
61 W. D. Cornell, P. Cieplak, C. I. Bayly, I. R. Gould, K. M. Merz, Jr., D. M. Ferguson, D. C. Spellmeyer, T. Fox, J. W. Caldwell and P. A. Kollman, *J. Am. Chem. Soc.*, 1995, **117**, 5179–5197.
62 I. G. Tironi, R. Sperb, P. E. Smith and W. F. van Gunsteren, *J. Chem. Phys.*, 1995, **102**(13), 5451–5459.
63 S. Hummer, G. Garde, A. E. Garcia, M. E. Paulaitis and L. R. Pratt, *J. Phys. Chem. B*, 1998, **102**(51), 10 469–10 482.
64 B. M. Pettitt and P. J. Rossky, *J. Chem. Phys.*, 1986, **84**(10), 5836–5844.
65 L. X. Dang and B. M. Pettitt, *J. Chem. Phys.*, 1987, **86**(11), 6560–6561.
66 L. X. Dang and B. M. Pettitt, *J. Am. Chem. Soc.*, 1987, **109**, 5531–5532.
67 L. X. Dang and B. M. Pettitt, *J. Phys. Chem.*, 1990, **94**, 4303–4308.
68 J. K. Buckner and W. L. Jorgensen, *J. Am. Chem. Soc.*, 1989, **111**, 2507–2516.
69 J. S. Bader and D. Chandler, *J. Phys. Chem.*, 1992, **96**, 6423–6427.
70 G. Hummer, D. M. Soumpasis and M. Neumann, *Mol. Phys.*, 1993, **81**(5), 1155–1163.
71 G. Hummer, L. R. Pratt and A. E. García, *J. Phys. Chem. A*, 1998, **102**, 7885–7895.
72 U. Essmann, L. Perera, M. L. Berkowitz, T. Darden, H. Lee and L. G. Pedersen, *J. Chem. Phys.*, 1995, **103**(19), 8577–8593.
73 T. Werder, J. H. Walther, R. Jaffe, T. Halicioglu, F. Noca and P. Koumoutsakos, *Nano Lett.*, 2001, **1**(12), 697–702.
74 M. J. de Ruijter, T. D. Blake and J. De Coninck, *Langmuir*, 1999, **15**, 7836–7847.